Fate of the quasicondensed state for bias-driven hard-core bosons in one dimension

T. O. Puel [1,2,*] Stefano Chesi [3,4,†] Stefan Kirchner [5,6,‡] and P. Ribeiro [7,3,§]

[1]*Department of Physics, Zhejiang Institute of Modern Physics, Zhejiang University, Hangzhou, Zhejiang 310027, China*
[2]*Department of Physics and Astronomy, University of Iowa, Iowa City, Iowa 52242, USA*
[3]*Beijing Computational Science Research Center, Beijing 100193, China*
[4]*Department of Physics, Beijing Normal University, Beijing 100875, China*
[5]*Department of Electrophysics, National Yang Ming Chiao Tung University, Hsinchu 30010, Taiwan*
[6]*Center for Emergent Functional Matter Science, National Yang Ming Chiao Tung University, Hsinchu 30010, Taiwan*
[7]*CeFEMA, Instituto Superior Técnico, Universidade de Lisboa Avenue Rovisco Pais, 1049-001 Lisboa, Portugal*

(Received 14 May 2022; accepted 23 February 2023; published 9 March 2023)

Bosons in one dimension display a phenomenon called quasicondensation where correlations decay in a power-law fashion. We study the fate of this quasicondensed state in an open-system setup where two macroscopic leads, held at different chemical potentials, drive the system far away from equilibrium. For generic leads, we find that a finite bias destroys the quasicondensed state and the system exhibits exponential-decay correlations and subleading power-law corrections that are bias dependent. Near the equilibrium, we found a diverging correlation length and determine the critical properties, including the critical scaling form of the correlations. Also, we contrast our findings against the fate of quasicondensation in thermal equilibrium and discuss the special case of reflectionless coupling where the quasicondensation survives out of equilibrium. This exactly solvable interacting nonequilibrium system has the remarkable property that the near-equilibrium state cannot be obtained within linear response. These results aid in unraveling the enigmatic properties spawned by strong interactions once liberated from equilibrium constraints.

DOI: 10.1103/PhysRevB.107.125122

The properties of states of matter far from thermal equilibrium and their relation to their equilibrium counterparts have become a topical issue of quantum matter research. In equilibrium, it has long been recognized that thermodynamic phases of low-dimensional systems are generally suppressed, due to the enhanced role of quantum fluctuations. This understanding rests, at least, in part on the range of analytical methods that are available for one-dimensional (1D) systems. For 1D hard-core bosons (HCB) this amounts to a phenomenon commonly referred to as quasicondensation where instead of a macroscopic occupation of the condensate wave function, the number of bosons in the ground-state increases as $\sqrt{N_b}$, where N_b is the total number of bosons. Quasicondensation is accompanied by off-diagonal quasi-long-range order, i.e., power-law decay of correlations that characterizes the quasicondensed state. First discovered for homogeneous systems [1,2], quasicondensed states of 1D HCB were shown to be ubiquitous, arising in the presence of harmonic trapping [3], periodic [4–6], and even quasiperiodic potentials [7]. The emergence of dynamic quasicondensation has also been observed in some nonequilibrium closed systems [8–10]. On the other hand, whereas quasicondensation appears to be a persistent feature of 1D HCB, its fate in open systems far from equilibrium has so far not been addressed.

This question is of significant interest as the relation of closed vs open nonequilibrium steady states (NESS) is highly nontrivial. Systems with identical equilibrium behavior can deviate drastically as, e.g., the involved symmetries differ [11,12]. Among possible nonequilibrium setups, transport configurations where the 1D systems are coupled to external reservoirs at different thermodynamic potentials are of great practical and theoretical relevance. For open quantum spin chains in the presence of a bias, it was recently shown that new behavior can emerge, which is absent in equilibrium [13,14]. There, the ordered state is robust to small applied biases but transitions discontinuously to the disordered state at large bias, through a mixed order phase transition. Interestingly, at that transition, the correlation length diverges. In contrast to the gapped ordered state of such spin chains, the equilibrium quasicondensed state is gapless, thus, its response to any nonequilibrium drive might qualitatively differ [15].

These considerations motivate us to investigate a system of HCB in the presence of an applied bias and, in particular, address the fate of the quasicondensed state. Naturally, considerable attempts have been made to extend the analytical methods, available to one-dimensional equilibrium systems to both closed and open systems far from equilibrium. For the closed case, these approaches include hydrodynamic methods for integrable models and generalized conformal field theory techniques [16,17] for nonintegrable ones. Approaches based on generalized Boltzmann-type equations [18–20] were

*tharnier@me.com
†stefano.chesi@csrc.ac.cn
‡stefan.kirchner@correlated-matter.com
§pedrojgribeiro@tecnico.ulisboa.pt

developed for dealing with open system dynamics. Of particular relevance to the present paper, is the extension of the bosonization technique to nonequilibrium setups, pioneered in Refs. [21–23]. Gutman *et al.* have shown that correlation functions, of interacting one-dimensional electrons, can be expressed through the asymptotics of Toeplitz determinants for imposed nonequilibrium electron distribution functions. Similar considerations also apply to the bosonic Tonks-Girardeau gas [23].

Here, we obtain the steady-state properties of a chain of hard-core bosons coupled at its ends to leads in the wideband limit. We show that the quasicondensed state is unstable towards an applied bias and characterize the ensuing NESS in terms of its single-particle equal-time correlators. We analyze the correlation length divergence in terms of the bias and determine how the quasi-long-range order is restored. It is demonstrated that there are power-law corrections to the exponential decay, which depend on the bias in a nonanalytic way once the thermodynamic limit is taken. As transport setups can now be readily engineered in confined ultracold atomic systems [24–26], a thorough understanding of quasicondensation in open systems far from equilibrium is timely and topical. Such an understanding might also shed new light on the similarities, and differences, between nonequilibrium transport in cold atoms and condensed-matter setups.

I. MODEL AND METHOD

We consider a tight-binding chain of HCB of size L coupled to reservoirs at its edges, modeled by the Hamiltonian $\mathcal{H} = \mathcal{H}_C + \sum_l (\mathcal{H}_l + \mathcal{H}_{C,l})$, where $\mathcal{H}_C = -J \sum_{\langle r,r'\rangle} \hat{b}_r^\dagger \hat{b}_{r'}$. HCB at the rth site are created (destroyed) by the operators $\hat{b}_r^\dagger$ ($\hat{b}_r$), which fulfill the commutation relations $[\hat{b}_r, \hat{b}_{r'}^\dagger] = \delta_{r,r'}(1 - 2\hat{b}_r^\dagger \hat{b}_r)$. Each of the two reservoirs $\mathcal{H}_l$ ($l = L, R$) is a semi-infinite chain of HCB with hopping strength J_l and chemical potential μ_l, held at zero temperature. In the following, we will use $\mu = (\mu_L + \mu_R)/2$ and $V = \mu_L - \mu_R$. As shown in Fig. 1(a), the reservoirs are coupled (through $\mathcal{H}_{C,l}$) to the very left ($r_L \equiv 1$) and right site ($r_R \equiv L$) of the chain, with coupling strength $J_{C,l}$. In the following we make the simplifying assumption that the bandwidths of the reservoirs J_l, are much larger than all other energy scales (wideband limit). In this limit, the coupling to each reservoir l is completely determined by $\Gamma_l = \pi J_l^2 \rho_l$, the hybridization energy scale, where ρ_l's are the local densities of states of the reservoirs, taken to be energy independent.

The Hamiltonian $\mathcal{H}$ possesses a fermionic representation which can be obtained through the Jordan-Wigner mapping [27], $\hat{b}_r^\dagger = \exp(i\pi \sum_{r'=1}^{r-1} \hat{c}_{r'}^\dagger \hat{c}_{r'}) \hat{c}_r^\dagger$, where $\hat{c}_r^\dagger$ ($\hat{c}_r$) creates (annihilates) a spinless fermion at site r. This yields a metallic chain in contact with baths of spinless fermions held at chemical potentials $\mu_{l=L,R}$. As the Jordan-Wigner-transformed Hamiltonian is quadratic in its fermionic degrees of freedom, the nonequilibrium system admits an exact solution in terms of single-particle quantities. Thus, we employ the nonequilibrium Green's function formalism to compute correlation functions and related observables. Steady-state observables can be obtained from the single-particle correlation-function matrix $\boldsymbol{\chi} \equiv \langle \hat{\boldsymbol{\Psi}} \cdot \hat{\boldsymbol{\Psi}}^\dagger \rangle$, with $\hat{\boldsymbol{\Psi}}^\dagger = (\hat{c}_1^\dagger, \ldots, \hat{c}_N^\dagger)$, which, in turn,

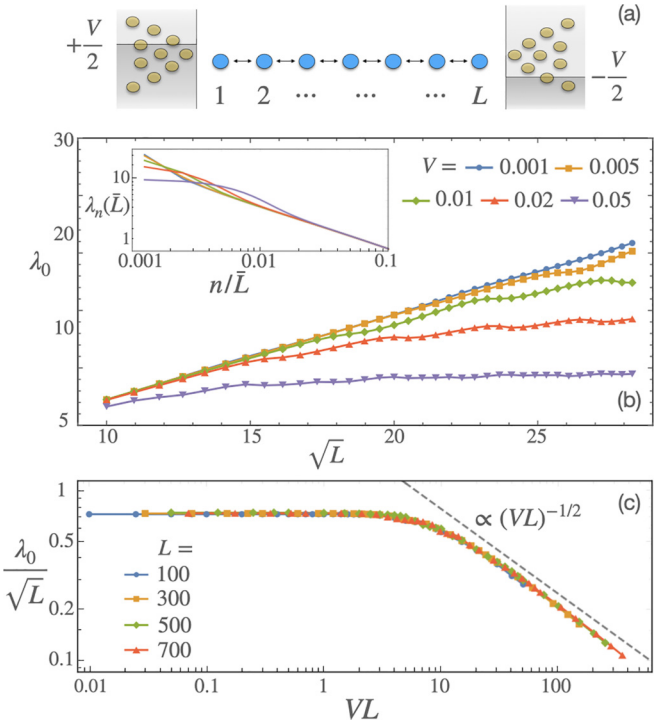

FIG. 1. (a) Sketch of the HCB chain coupled to bosonic reservoirs. (b) Maximum natural-orbital occupation λ_0 as function of $\sqrt{L}$ for several chemical potential profiles V. The inset shows the occupations $\lambda_n(\bar{L})$ for $\bar{L} = 800$. (c) Scaling collapse of $\lambda_0 L^\beta \times VL^\alpha$ for different system sizes L. Best fits to the data are compatible with $\alpha = 1$ and $\beta = -1/2$.

is obtained from the Keldysh Green's function as described in Ref. [14]. The method allows us to obtain mean values of quadratic observables $\hat{O} = \hat{\boldsymbol{\Psi}}^\dagger \cdot \boldsymbol{O} \cdot \hat{\boldsymbol{\Psi}}$ from the relation $\langle \hat{O} \rangle = -\mathrm{tr}[\boldsymbol{O} \cdot \boldsymbol{\chi}]$. Finally, the bosonic one-body density matrix $\rho^B_{r,r'} = \langle \hat{b}_r^\dagger \hat{b}_{r'} \rangle$ can be computed from the fermionic one, $\rho^F_{r,r'} = \langle \hat{c}_r^\dagger \hat{c}_{r'} \rangle = \delta_{r,r'} - \chi_{r',r}$, using the approach described, e.g., in Ref. [28]. One finds

$$\rho^B_{r,r'} = \frac{1}{2} \det \left[\sum_{i,j=1}^{r-r'} \left(2\rho^F_{j+r',i+r'-1} - \delta_{j+1,i} \right) |i\rangle\langle j| \right] \quad (1)$$

for $r > r'$, and $\rho^B_{r',r} = (\rho^B_{r,r'})^*$. The eigenvectors of the matrix ρ^B define the natural orbitals and the corresponding eigenvalues λ_n their occupations. Taking the λ_n in decreasing order, the quasicondensed state is characterized by a macroscopic occupation of its lowest orbital, $\lambda_0 \propto \sqrt{N_b}$, where $N_b \propto L$ in the macrocanonical ensemble [1,2]. On general grounds, the occupations behave as $\lambda_n(L \to \infty) \propto n^{-1/2}$ in the thermodynamic limit at zero temperature (T). In equilibrium, quasicondensation is destroyed at nonzero temperature or in the presence of a localization potential.

II. RESULTS

Figure 1(b) shows the occupation of the lowest natural orbital λ_0 as a function of L in the NESS obtained for $V \neq 0$. In that case, λ_0 saturates with L, thus, implying that the quasi-condensed state only exists for $V = 0$. Nevertheless,

the scaling $\lambda_0 \propto \sqrt{L}$ is still observed before the saturation scale is attained. The inset shows the scaling of $\lambda_n(L)$ with n, having fixed $L = 800$. For sufficiently large values of n, we find $\lambda_n \propto n^{-1/2}$, whereas, for small values, saturation ensues at finite values of V. These findings establish that V is a relevant perturbation, such as T is in equilibrium. However, as will be demonstrated, the NESS is fundamentally different from the finite-temperature state: Its critical behavior, characterizing the vicinity of the unstable quasicondensation fixed point along the V direction, turns out to be different from the equilibrium case. Figure 1(c) depicts the scaling collapse of $\lambda_0 L^{\beta}$ versus VL^{α} for different values of L. Best fits to the data are compatible with $\alpha = 1$ and $\beta = -1/2$, which turn out to be the exact exponents, see below. For small VL ($VL \leqslant 2$), this recovers the $V = 0$ result $\lambda_0 \propto \sqrt{L}$, whereas for VL large, $\lambda_0 \propto V^{-1/2}$.

We now turn to the description of the NESS. For large system sizes, the state in the middle of the chain displays translational invariance and ρ^B becomes diagonal in momentum space. In this case, the natural orbitals coincide with the momentum states. We label their occupations by $\lambda_n(L \gg 1) \to n_k^B$. Figure 2(a) depicts the Fourier transform of the bosonic occupation in momentum space in the middle of the chain. Here, we also compare numerical results (plot markers) for finite $L = 800$ to analytical predictions (solid lines) valid for small V, discussed in detail below. Clearly, both coincide for sufficiently small V. The effect of V is twofold: (i) the $1/\sqrt{k}$ divergence of n_k^B at $V = 0$ gets regularized at a scale $1/\sqrt{V}$, and the curve acquires a characteristic width to which we refer as ξ^{-1}, illustrated in Fig. 2(a) (for the blue curve); (ii) the maximum value of the peak shifts to finite momentum, denoted as φ. Both quantities together with a power-law exponent ν [see Eq. (2) below] characterize the departure from equilibrium of a quasicondensate state, which is induced via a particle number bias.

A proper definition of ξ^{-1} and φ is given in terms of the asymptotic dependence of the bosonic correlation function. In the limit $r - r' \to \infty$,

$$\rho^B_{r-r'} \simeq E e^{-|r-r'|/\xi - i(r-r')\varphi}(r - r')^{-\nu}, \tag{2}$$

where E is a constant. As we will discuss in detail, this general dependence follows from taking the thermodynamic limit, which brings $\rho^B_{r,r'}$ to the form given in Eq. (3) and allows us to apply the Fisher-Hartwig conjecture for Toeplitz matrices. Interestingly, the asymptotic behavior of $\rho^B_{r-r'}$ displays power-law corrections on top of the exponential decay, where ν is a complex-valued critical exponent. The behavior of ξ^{-1} and φ with V, obtained by fitting the numerical $\rho^B_{r,r'}$ to Eq. (2), is given by the green dots in Figs. 2(b) and 2(c), respectively. These results agree (within the error bars) with our analytical formulas, given below. Furthermore, in Figs. 2(d) and 2(e) we examine the power-law exponent ν. Although a finite value of $\nu = 1/2$ is expected in equilibrium when $\xi^{-1} = \varphi = 0$, our analytic results show that ν is discontinuous at $V = 0$ and assumes a V-independent constant for any nonvanishing value of the bias, e.g., $V \neq 0$. This discontinuity only occurs in the thermodynamic limit. Our numerical results show that ν indeed remains constant for a finite chain at a sufficiently large V but will acquire strong finit- size corrections as V is reduced, see Figs. 2(d) and 2(e). Power-law corrections on top of the exponential decay are hard to determine based on Eq. (1). Results shown in both panels (d) and (e) are, therefore, obtained by a numerical evaluation of Eq. (3) below, that allows accessing much larger system sizes. Nevertheless, we confirmed (see Appendix B 3) that the numerical results obtained with Eq. (1) are fully compatible with the analytic asymptotic form.

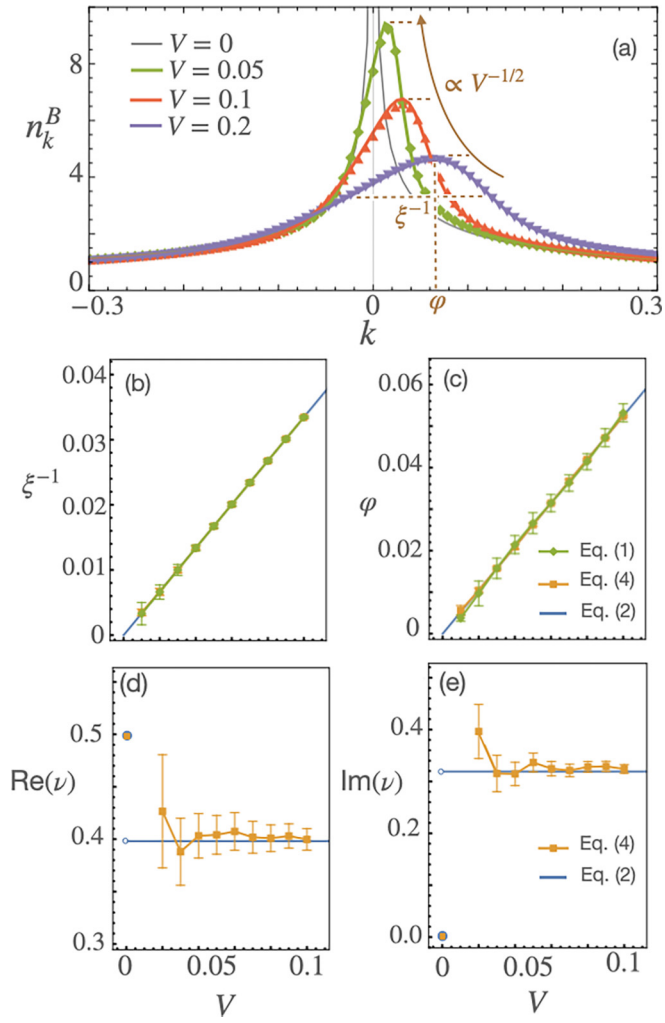

FIG. 2. (a) Momentum distribution of the one-body density matrix for various values of the bias V. Comparison between numerical and analytic results for: (b) The exponential decay length ξ^{-1}; (c) The momentum displacement φ; (d) The real part of the power-law decay exponent ν, defined in Eq. (2); (e) The imaginary part of ν. Direct evaluation of Eq. (1) (green) is contrasted with results based on the asymptotic form in Eq. (3) (orange) and with the analytic expression of Eq. (2) (blue).

These findings constitute the main nontechnical results of our paper. In what follows, we explain the method used to obtain our numerical results and derive Eq. (2), including an explicit expression for ξ, φ, and ν.

A. Single-particle correlations

The numerical evaluation of single-particle correlators is most conveniently performed in the fermionic representation

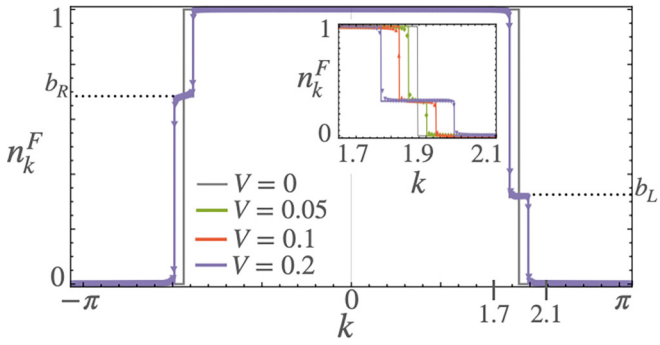

FIG. 3. Momentum distribution function of the Jordan-Wigner fermions for $V = 0$ and $V = 0.2$ which has been calculated in Ref. [30] and is reproduced here for clarity, as it enables one to determine the bosonic distribution function far from equilibrium. Insert shows the double-step structure for different values of V. The step width is V/v_{F} and the heights, b_L and b_R, depend on the chain-lead couplings.

which leads to the non-Hermitian single-particle operator $\boldsymbol{K} = \boldsymbol{H}_{\mathrm{C}} - i\sum_{l=L,R}\boldsymbol{\gamma}_l$, with the Hamiltonian of the chain $\boldsymbol{H}_{\mathrm{C}} = -J\sum_{r=1}^{L-1}|r\rangle\langle r+1| + \mathrm{H.c.}$, and where $|r\rangle$ is a single-particle state. The hybridization matrices of each reservoir are $\boldsymbol{\gamma}_l = \Gamma_l|r_l\rangle\langle r_l|$. For the fermionic system, the single-particle correlation-function matrix $\boldsymbol{\chi}$ can be obtained using nonequilibrium Green's function methods (see Refs. [14,28,29]). The resulting expression is explicitly given in Appendix A 1 in terms of the eigenvalues and eigenvectors of $\boldsymbol{K}$. The matrix $\boldsymbol{\chi}$ is then used to numerically evaluate the bosonic one-body density matrix as in Eq. (1).

Alternatively, one can obtain the fermionic one-body density matrix analytically. Noticing that in the bulk of an infinite chain the Fourier transform of $\rho^F_{r,r'} = \rho^F_{r-r'}$ becomes the momentum occupation number n_k^{F}, an explicit expression of n_k^{F} can be obtained when the energy dispersion is represented by a linear k dependence near the Fermi points, provided $V \ll J$ [30]. In this case, n_k^{F} assumes the double-step structure illustrated in Fig. 3 (see Ref. [30] and Appendix A 2). Each double-step has a width of V/v_{F} with the Fermi velocity $v_{\mathrm{F}} = 2J\sin(k_{\mathrm{F}})$, and is centered around the average Fermi momentum $k_{\mathrm{F}} = \arccos[-(\mu_L+\mu_R)/4J]$. The occupations of the left (right), b_R (b_L) steps depend on the couplings to the reservoirs and on the Fermi velocity [30]. For the special case of reflectionless leads, i.e., $b_L = 1\,(=0)$ and $b_R = 0\,(=1)$ for $V > 0\,(<0)$, the double-step structure no longer arises. In this case, n_k^{F} becomes a momentum-displaced Fermi function which leads to a qualitative difference for n_k^B as discussed below.

Expressed in terms of n^{F}, the asymptotic limit of ρ^B assumes the form of a Toeplitz matrix (see Appendix B1). Explicitly, from Eq. (1) one finds

$$\rho^B_{r-r'} = \frac{1}{2}\det\left[\sum_{i,j=1}^{r-r'}\int\frac{dk}{2\pi}\left(2n_k^{\mathrm{F}}-1\right)e^{ik(i-j-1)}|i\rangle\langle j|\right]. \quad (3)$$

The result given in Eq. (2) was obtained using the Fisher-Hartwig conjecture for Toeplitz matrices, giving the asymptotic behavior of Eq. (3) in the limit $r - r' \to \infty$ (see Appendix B). The correlation length ξ^{-1}, the displacement momentum φ, and the real and imaginary parts of the power-law exponent ν are explicitly given by

$$\xi^{-1} = -\frac{1}{2\pi}\frac{|V|}{v_{\mathrm{F}}}\log(|1-2b_L||1-2b_R|),$$

$$\varphi = \frac{1}{4}\frac{V}{v_{\mathrm{F}}}[\mathrm{sgn}(1-2b_L) - \mathrm{sgn}(1-2b_R)],$$

$$\mathrm{Re}(\nu) = \frac{1}{2} - \frac{1}{2\pi^2}[\log^2(|1-2b_L|) + \log^2(|1-2b_R|)],$$

$$\mathrm{Im}(\nu) = \frac{\mathrm{sgn}(V)}{2\pi}\left[\frac{\log(|1-2b_R|)}{\mathrm{sgn}(1-2b_R)} - \frac{\log(|1-2b_L|)}{\mathrm{sgn}(1-2b_L)}\right].$$

The constant E in Eq. (2) can also be obtained explicitly as a function of V/v_{F}, b_L and b_R, and is given in Appendix B 2.

III. DISCUSSION

The numerical and analytical results presented so far allow us to address the fate of quasicondensation at finite bias and contrast it with what happens when turning on the heat at zero bias. For generic leads, both nonzero V and nonzero T are relevant perturbations which destroy quasicondensation and lead to an exponential decay of correlations with distance. This is reflected in similar finite-size scaling behavior of λ_0 vs V, see Fig. 1(c), and T, obtained in Ref. [31]. There are, however, clear differences in how this destruction occurs in both cases. Although the equilibrium correlations at finite T decay exponentially, the out-of-equilibrium decay as we have shown is characterized by additional power-law corrections on top of the exponential decay, see Eq. (2). These differences will be most apparent at the short-to-intermediate range where these power-law corrections are sizable and are, e.g., also reflected in the behavior of the mutual information of the Jordan-Wigner fermions [30,32]. Yet another difference between the two cases concerns the steady state realized in the $V \to 0$ limit. In the thermodynamic limit $|V| \to 0^+$ results in a divergence of ξ, thus, recovering the quasicondensed state. However, the power-law scaling characterizing this state depends on the coupling to the leads and is, in general, different from $\nu = 1/2$ observed in equilibrium.

This should be contrasted with the case of ideal reflectionless leads, where $\xi^{-1} = 0$ and $\nu = 1/2$ for any V. Here, the form of n_k^{F} corresponds to that in the equilibrium state with a shift in k proportional to the applied bias, $n_k^B = n^{B(\mathrm{Eq.})}_{(k-\varphi)}$. This implies that, in this case, the quasicondensed phase is robust to the applied bias and the most populated natural orbital acquires a finite momentum $k = \varphi$. Thus, the critical properties away from equilibrium depend crucially on the system-lead couplings. This is in stark contrast to what happens in equilibrium where the thermal state is insensitive to the details of the coupling to the environment.

An important direction concerning future work is the stability of our findings with respect to interactions. It will be interesting to address the effect of a relaxation of the hard-core constraint and the resulting softening of occupation numbers. Another open question regards the role of dimensionality. True condensation occurs in two- and higher-dimensional systems in equilibrium, but its fate out of equilibrium has so

far remained unclear. In particular, it would be worthwhile to understand if this out-of-equilibrium steady state is fundamentally different from its thermal counterpart, in analogy to what happens in 1D.

ACKNOWLEDGMENTS

We thank Beijing Computational Science Research Center (CSRC) for providing access to the Tianhe-2JK cluster where the calculations were performed. S.C. acknowledges support from the Innovation Program for Quantum Science and Technology (Grant No. 2021ZD0301602), the National Science Association Funds (Grant No. U2230402), and the National Natural Science Foundation of China (Grants No. 11974040 and No. 12150610464). S.K. acknowledges support by the National Science and Technology Council, Taiwan (Grant No. MOST 111-2634-F-A49-007), the Featured Area Research Center Program within the framework of the Higher Education Sprout Project by the Ministry of Education (MOE) in Taiwan and the Yushan Fellowship Program of the MOE Taiwan. P.R. acknowledges support by FCT through Grant No. UID/CTM/04540/2019 and by the QuantERA II Programme that has received funding from the European Union's Horizon 2020 research and innovation programme under Grant Agreement No 101017733.

APPENDIX A: FERMIONIC QUANTITIES

1. Single-particle correlation matrix

To obtain the single-particle correlation matrix, we assume that $\boldsymbol{K}$ is diagonalizable, having right and left eigenvectors $|\alpha\rangle$ and $\langle\tilde{\alpha}|$ with associated eigenvalues λ_α. The single-particle correlation-function matrix $\boldsymbol{\chi}$ is then given by [14,28,29]

$$\boldsymbol{\chi} = \frac{1}{2} + \sum_{l=L,R}\sum_{\alpha\beta} |\alpha\rangle\langle\beta|\langle\tilde{\alpha}|[\gamma_l I_l(\lambda_\alpha, \lambda_\beta^*) - \hat{\gamma}_l I_l(-\lambda_\alpha, -\lambda_\beta^*)]|\tilde{\beta}\rangle, \tag{A1}$$

where

$$I_l(z, z') = -\frac{1}{\pi}\frac{g(z-\mu_l) - g(z'-\mu_l)}{z - z'}, \tag{A2}$$

with $g(z) = \ln(-i\ \mathrm{sgn}[\mathrm{Im}(z)]z)$.

The numerical results in the main text were obtained by performing an exact diagonalization of the matrix $\boldsymbol{K}$ as explicitly given in the main text, and evaluating Eq. (A1) with the chemical potentials of the leads entering through Eq. (A2).

2. Fermionic-particle density

The fermionic-particle density, computed in Ref. [30], is

$$n_k^{\mathrm{F}} = \begin{cases} 1, & 0 < k < \theta_1, \\ b_L, & \theta_1 < k < \theta_2, \\ 0, & \theta_2 < k < \theta_3, \\ b_R, & \theta_3 < k < \theta_4, \\ 1, & \theta_4 < k < 2\pi, \end{cases} \tag{A3}$$

with the momenta where n^{F} is discontinuous given by

$$\theta_1 = k_F - \frac{\Delta}{2}, \quad \theta_2 = k_{\mathrm{F}} + \frac{\Delta}{2}, \quad \theta_3 = 2\pi - k_{\mathrm{F}} - \frac{\Delta}{2}, \quad \theta_4 = \pi - k_{\mathrm{F}} + \frac{\Delta}{2}, \tag{A4}$$

where $\Delta = V/v_{\mathrm{F}}$. The values of b_R and b_L are obtained from

$$b_R = -\frac{(1-\gamma_L)}{\gamma_L\gamma_R - 1}, \quad b_L = \gamma_R b_R, \tag{A5}$$

in which

$$\gamma_l = \frac{(\Gamma_l/J)^2 - (2/J)\sin(k_F)\Gamma_l + 1}{(\Gamma_l/J)^2 + (2/J)\sin(k_F)\Gamma_l + 1}, \quad l = L, R. \tag{A6}$$

APPENDIX B: TOEPLITZ DETERMINANT AND FISHER-HARTWIG CONJECTURE

In the thermodynamic limit, the matrix $\rho^{\mathrm{F}}_{i,j}$ for i and j in a segment in the middle of the chain becomes translationally invariant and assumes the Toeplitz form $\rho^{\mathrm{F}}_{i,j} = \rho^{\mathrm{F}}_{i-j}$. Its asymptotic behavior is given by Eq. (3). Physical quantities related to ρ^{F}, thus, require the evaluation of the determinant of Toeplitz matrices, which we perform in the following using the Fisher-Hartwig conjecture.

1. Toeplitz matrix

Consider a Toeplitz matrix $T_n[\phi] = \sum_{q,l=1}^{n} \phi_{q-l}|q\rangle\langle l|$, generated by a function of the form

$$\phi_{q-l} = \int_0^{2\pi} \frac{d\theta}{2\pi}\phi(\theta)e^{-i(q-l)\theta}, \tag{B1}$$

where the nonanalyticities of $\phi(\theta)$ are assumed to consist only of discontinuities. In this case, it can be decomposed in the form [33]

$$\phi(\theta) = b(\theta)\prod_{r=1}^{R} e^{-i\beta_r[\pi-(\theta-\theta_r)]}, \tag{B2}$$

where θ_r's are the discontinuity points. Comparing Eq. (3) in the main text and Eq. (B1) we identify

$$\phi(\theta) \to \phi(k) = \left[1 - 2n_k^{\mathrm{F}}\right]e^{-ik}, \tag{B3}$$

with n_k^{F} given in Eq. (A3). The discontinuities θ_r of n_k^{F} are defined in Eq. (A5) for $r = 1$–4. In order to identify the coefficients β_r, we impose

$$e^{\ln[1-2n_k^F]-ik} = e^{V_0 - i\sum_r \beta_r[\pi-(k-\theta_r)]}, \tag{B4}$$

where we defined $b(k) \equiv \exp[V_0]$ in Eq. (B2), to be valid for each of the continuous regions of Eq. (A3). In between the regions, the exponents of both sides have to coincide up to a constant $2\pi i n_j$ with $n_j \in \mathbb{Z}$ defined in region j. Note that there are only four regions since $0 < k < \theta_1$ and $\theta_4 < k < 2\pi$ are connected by periodicity.

Equating the coefficients multiplying k on both sides we obtain

$$\sum_{r=1}^{4}\beta_r = -1, \tag{B5}$$

which leaves us with only three independent variables, n_1, n_2, and n_3, that must satisfy

$$\beta_1 = n_2 - n_1 + \frac{i\log(1-2b_R)}{2\pi} + \frac{1}{2}, \tag{B6}$$

$$\beta_2 = n_3 - n_2 - \frac{i\log(1-2b_R)}{2\pi}, \tag{B7}$$

$$\beta_3 = n_4 - n_3 + \frac{i\log(1-2b_L)}{2\pi}, \tag{B8}$$

$$\beta_4 = -1 - \beta_1 - \beta_2 - \beta_3, \tag{B9}$$

and

$$V_0 = \frac{\Delta}{2\pi}[\log(1-2b_L) + \log(1-2b_R)] - i[\pi + 2(n_1 - n_3 - 1)k_F - \Delta(n_1 - n_2 + n_3 - n_4 + 1)]. \tag{B10}$$

The values of the integers n_j are determined in the following, using the formulation of the Fisher-Hartwig conjecture in Ref. [33].

2. Fisher-Hartwig conjecture

The Fisher-Hartwig conjecture states that

$$\det T_\ell[\phi] \simeq E e^{\ell V_0} \ell^{-\sum_r {\beta_r}^2}, \quad \ell \to \infty, \tag{B11}$$

where E is an ℓ-independent constant evaluated below. In the following, we chose the values of n_j that maximizes Eq. (B11). The dependence of V_0 on n_1, n_2, and n_3 does not affect the absolute value of $\det T_\ell$. Therefore, the determination of n_j is obtained by minimizing $\mathrm{Re}[\sum_r {\beta_r}^2]$. The result depends on $\mathrm{sgn}(\Delta)$ and whether $(1-2b_{L/R})$ is positive or negative. After this procedure, the expressions for β_j write

$$\beta_1 = -\frac{1}{2} - i\,\mathrm{sgn}(\Delta)\frac{\mathrm{sgn}(1-2b_R)\log(|1-2b_R|)}{2\pi}, \tag{B12}$$

$$\beta_2 = -\frac{1}{2} - \beta_1, \tag{B13}$$

$$\beta_3 = -i\,\mathrm{sgn}(\Delta)\frac{\mathrm{sgn}(1-2b_L)\log(|1-2b_L|)}{2\pi}, \tag{B14}$$

$$\beta_4 = -1 - \beta_1 - \beta_2 - \beta_3, \tag{B15}$$

and

$$V_0 = \frac{|\Delta|}{2\pi}\log(|1-2b_L||1-2b_R|), + i\left[\pi + \frac{\Delta}{4}[\mathrm{sgn}(1-2b_L) - \mathrm{sgn}(1-2b_R)]\right]. \tag{B16}$$

Using Ref. [33], it follows that the amplitude E in Eq. (B11) is obtained from the expression,

$$E = \prod_{1\leqslant r\neq s\leqslant 4}(1-e^{i(\theta_s-\theta_r)})^{\beta_r\beta_s}\prod_{k=4}^{4} G(1+\beta_k)G(1-\beta_k), \tag{B17}$$

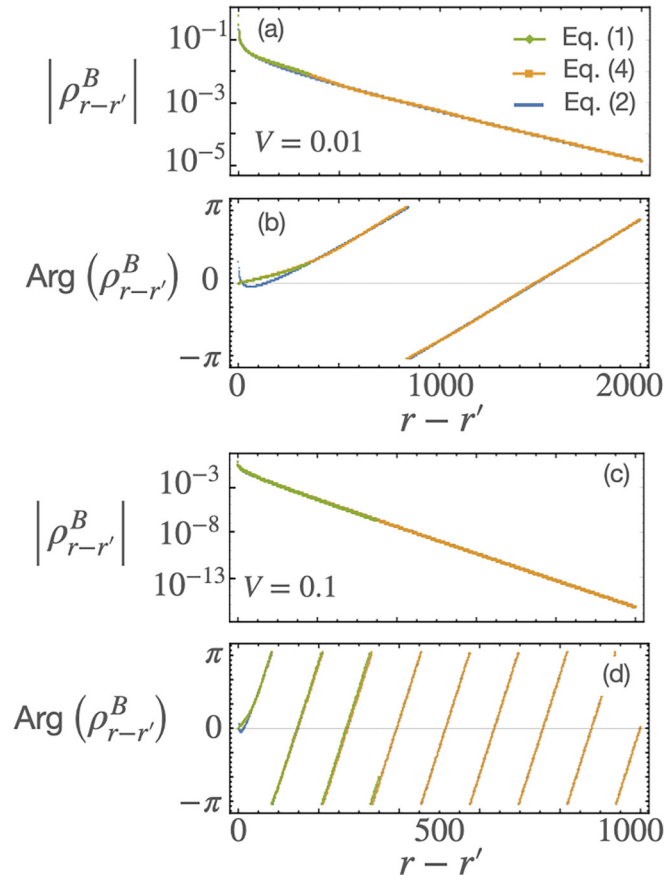

FIG. 4. (a) and (b) are the particle density for $V = 0.01$, whereas (b) and (c) are the particle density for $V = 0.1$.

where G is the Barnes G function,

$$G(1+z) = (2\pi)^{z/2}e^{-(z+(\gamma+1)z^2)/2}\prod_{k=1}^{\infty}\left(\frac{1+z}{k}\right)^k e^{-z+z^2/(2k)}, \tag{B18}$$

and γ is the Euler constant.

3. Bosonic single-particle matrix

Recasting the results of the previous sections, we evaluate Eq. (3) in the main text and obtain

$$\rho^B_{|r-r'|} = \frac{E}{2}e^{|r-r'|V_0}|r-r'|^{-\nu}. \tag{B19}$$

The correlation function and the momentum shift, defined in the main text, can be identified as $V_0 = -\xi^{-1} + i\varphi$ and $\nu = \sum_r {\beta_r}^2$. The corresponding expressions are given explicitly in the main text.

Figure 4 shows a real-space comparison of the asymptotic result, obtained here using the same color coding as in the main text. Although the results based on the different methods are compatible with each other for small values of V, it is difficult to access the asymptotic regime for large $r - r'$ using Eq. (1). This difficulty explains the growing error bars and why we were not able to provide full numerical results of small V in Fig. 2.

[1] A. Lenard, J. Math. Phys. **5**, 930 (1964).
[2] H. G. Vaidya and C. A. Tracy, Phys. Rev. Lett. **42**, 3 (1979).
[3] M. Rigol and A. Muramatsu, Phys. Rev. A **70**, 031603(R) (2004).
[4] M. D. Girardeau, E. M. Wright, and J. M. Triscari, Phys. Rev. A **63**, 033601 (2001).
[5] T. Papenbrock, Phys. Rev. A **67**, 041601(R) (2003).
[6] P. J. Forrester, N. E. Frankel, T. M. Garoni, and N. S. Witte, Phys. Rev. A **67**, 043607 (2003).
[7] P. Ribeiro, M. Haque, and A. Lazarides, Phys. Rev. A **87**, 043635 (2013).
[8] M. Rigol and A. Muramatsu, Phys. Rev. Lett. **93**, 230404 (2004).
[9] L. Vidmar, J. P. Ronzheimer, M. Schreiber, S. Braun, S. S. Hodgman, S. Langer, F. Heidrich-Meisner, I. Bloch, and U. Schneider, Phys. Rev. Lett. **115**, 175301 (2015).
[10] P. Ribeiro, A. Lazarides, and M. Haque, Phys. Rev. Lett. **124**, 110603 (2020).
[11] P. C. Hohenberg and B. I. Halperin, Rev. Mod. Phys. **49**, 435 (1977).
[12] A. Mitra, S. Takei, Y. B. Kim, and A. J. Millis, Phys. Rev. Lett. **97**, 236808 (2006).
[13] M. M. Oliveira, P. Ribeiro, and S. Kirchner, Phys. Rev. Lett. **122**, 197601 (2019).
[14] T. O. Puel, S. Chesi, S. Kirchner, and P. Ribeiro, Phys. Rev. B **103**, 035108 (2021).
[15] P. Ribeiro, F. Zamani, and S. Kirchner, Phys. Rev. Lett. **115**, 220602 (2015).
[16] D. Bernard and B. Doyon, J. Stat. Mech. (2016) 064005.
[17] V. Alba, B. Bertini, M. Fagotti, L. Piroli, and P. Ruggiero, J. Stat. Mech. (2021) 114004.
[18] A. Levchenko, T. Micklitz, Z. Ristivojevic, and K. A. Matveev, Phys. Rev. B **84**, 115447 (2011).
[19] T. Micklitz and A. Levchenko, Phys. Rev. Lett. **106**, 196402 (2011).
[20] T. Micklitz, A. Levchenko, and A. Rosch, Phys. Rev. Lett. **109**, 036405 (2012).
[21] D. B. Gutman, Y. Gefen, and A. D. Mirlin, Phys. Rev. Lett. **101**, 126802 (2008).
[22] D. B. Gutman, Y. Gefen, and A. D. Mirlin, Phys. Rev. B **80**, 045106 (2009).
[23] D. B. Gutman, Y. Gefen, and A. D. Mirlin, J. Phys. A: Math. Theor. **44**, 165003 (2011).
[24] J.-P. Brantut, J. Meineke, D. Stadler, S. Krinner, and T. Esslinger, Science **337**, 1069 (2012).
[25] C.-C. Chien, S. Peotta, and M. Di Ventra, Nat. Phys. **11**, 998 (2015).
[26] S. Krinner, T. Esslinger, and J.-P. Brantut, J. Phys.: Condens. Matter **29**, 343003 (2017).
[27] E. Lieb, T. Schultz, and D. Mattis, Ann. Phys. (NY) **16**, 407 (1961).
[28] M. Rigol and A. Muramatsu, Phys. Rev. A **72**, 013604 (2005).
[29] T. O. Puel, S. Chesi, S. Kirchner, and P. Ribeiro, Phys. Rev. Lett. **122**, 235701 (2019).
[30] P. Ribeiro, Phys. Rev. B **96**, 054302 (2017).
[31] M. Rigol, Phys. Rev. A **72**, 063607 (2005).
[32] G. Vidal, J. I. Latorre, E. Rico, and A. Kitaev, Phys. Rev. Lett. **90**, 227902 (2003).
[33] E. L. Basor and K. E. Morrison, Linear Algebra Appl. **202**, 129 (1994).